

SLHC Upgrade of the ATLAS SCT Tracker

Y. Unno* (on behalf of the ATLAS SCT Upgrade Sensor Collaboration)
Institute of Particle and Nuclear Study, KEK, 1-1 Oho, Tsukuba 305-0801, Japan

Abstract

The LHC accelerators and detectors will be upgraded to the super LHC (SLHC) in two phases: in PHASE-I to the peak luminosities of $\sim 3 \times 10^{34} \text{ cm}^{-2} \text{ s}^{-1}$, and PHASE-II to $\geq 10 \times 10^{34} \text{ cm}^{-2} \text{ s}^{-1}$, to collect proton-proton collision data of $\sim 3000 \text{ fb}^{-1}$ per experiment. The complete inner trackers of the ATLAS detector will be replaced with new Silicon pixels in the inner part and new Silicon microstrip detectors in the outer part. The n-strips in the p-type material (“n-in-p”) microstrip sensors have been developed. The n-in-p sensor collects electrons, the faster signals, in the p-n junction side of the detector throughout its lifetime. Characterization of the wafer materials and the design of the strip sensors have advanced through the development of ATLAS05, ATLAS06, and ATLAS07 sensors. An n-in-p silicon microstrip sensor has emerged that tolerates bias voltage up to $\sim 1,000 \text{ V}$, in 150 mm diameter FZ wafers from industry.

PACS: 29.40.W; 81.40.W

Keywords: p-bulk; p-type; FZ; MCZ; Silicon; Microstrip; Irradiation; Radiation damage

1. Introduction

Operation of the Large Hadron Collider (LHC) started on 10th September 2008¹ [1]. The LHC is planned to collect proton-proton collisions to total $\sim 700 \text{ fb}^{-1}$ per experiment in 10 years, with luminosity of 10^{33} to the 10^{34} in the first 3 years of ramp-up and $1 \times 10^{34} \text{ cm}^{-2} \text{ s}^{-1}$ in each of the following 7 years. The physics goals of LHC are, e.g., the discoveries of either the Higgs boson or an alternative mechanism up to $\sim \text{TeV}$ energy range, new heavy electroweak vector bosons, W' , Z' , whose mass limit up to $\sim 5 \text{ TeV}/c^2$, new elementary particles associated with the super-symmetry (SUSY) to the mass limit up to $\sim 2.5 \text{ TeV}/c^2$. The Higgs boson is believed responsible for spontaneous symmetry breaking in the standard model (SM), and the others are associated with the physics beyond the SM.

Whatever is discovered will need much more study [3], e.g. clarifying the Lagrangian of the spontaneous symmetry breaking with precise measurement of parameters such as the Higgs boson's coupling to fermions and bosons with improved precision, and the self-coupling of the Higgs bosons. Some models beyond the SM predict more than one Higgs bosons and we need to explore full range of parameter space, e.g., in the minimal super-symmetric model (MSSM). If there is no Higgs boson, an alternate mechanism such as resonant and

* Corresponding author. Tel: +81 29 864 5791, fax: +81 29 864 2580. E-mail address: yoshinobu.unno@kek.jp (Y. Unno)

¹ On 19th September, during the commissioning of the main super-conducting dipole magnets in the sector 3-4 (without beam), a number of magnets were damaged in an incident that saw a large amount of Helium released into the tunnel, caused by a faulty electrical connection between two of the magnets [2].

non-resonant electroweak boson scattering in the TeV energy region is required. If SUSY particles are found, we need to measure their decay chain for identifying their structure. The statistics of LHC will be too low for this purpose. An integrated luminosity of $>3,000 \text{ fb}^{-1}$ per experiment is required to explore these possibilities. It is expected that the LHC will be upgraded to the super LHC (SLHC) to provide an instantaneous luminosity of $\geq 10^{35} \text{ cm}^{-2}\text{s}^{-1}$ [4].

2. Evolution of LHC to SLHC

In general, the peak luminosity of the LHC, L , is given by the formula

$$L = \frac{N_b^2 n_b f_r \gamma}{4\pi \epsilon_n \beta^*} F \quad (1)$$

where N_b is the number of particles per bunch [1.15×10^{11}], n_b the number of bunches [2808], f_r the revolution frequency [$1.12 \times 10^4 \text{ s}^{-1}$], γ the relativistic factor [7461], ϵ_n the normalized emittance [$3.75 \times 10^{-4} \text{ cm rad.}$], β^* the beta value at the interaction point [55 cm], and F the reduction factor due to the crossing angle [0.86]. The nominal values of the LHC of the $1 \times 10^{34} \text{ cm}^{-2}\text{s}^{-1}$ are given in the square brackets. Luminosity is limited to 40 % of the nominal until collimators are installed in the shutdown of 2010/11. The collimation scheme may yet limit the luminosity up to 60% of the nominal as $\beta^* \geq 80 \text{ cm}$ is required if the impedance is not tolerable.

To overcome these limitations and reach luminosity of $10^{35} \text{ cm}^{-2}\text{s}^{-1}$, a sequence of upgrades is planned for the accelerators, a PHASE- I upgrade during 2013-2015 and a PHASE-II from 2017. The major parameters to be upgraded are N_b and β^* , together with replacing the aging accelerator complex for reliable operation and higher current [5].

PHASE-I Upgrade:-- The goal of this upgrade is to increase the luminosity to $\sim 3 \times 10^{34}$ which is tolerable by the existing experiments without major detector upgrade. The inner triplet focusing magnets will be replaced in order to squeeze β^* to 25 cm and to ease collimation with enlarged aperture. The first stage proton linac will be replaced by a new one, Linac-4, for the ultimate current of the LHC with the N_b of 1.7×10^{11} .

PHASE-II Upgrade:-- Two new accelerators are to be built, the Low Power Superconducting Proton Linac (LPSPL) and the High Energy Proton Synchrotron (PS2), in order to achieve to deliver 2.2times the ultimate current for the LHC. Several schemes for the interaction points are being explored to achieve the SLHC luminosity [6]. The options include (1) to have a null collision angle ($F=1$) or (2) to have a large collision angle ($F<1$) but with a larger N_b in a longer bunch. There is a finite crossing angle of the two beams in a macro scale in either scheme. The null collision angle is achieved either by (1-1) the ‘‘Early Separation (ES)’’ scheme where separation magnets are placed inside the experiments, close to the interaction point, or (1-2) the ‘‘Full Crab Crossing (FCC)’’ scheme where the beam bunches are rotated with a ‘‘crab cavity’’ to make the null collision angle. The finite collision angle scheme is called the ‘‘Large Piwinski angle (LPA)’’ scheme. Typical parameters of the schemes are summarized in Table 1. A large number of pile-up events, 300 to 400, are expected at the start of the beam spill. A technique called ‘‘luminosity leveling’’ has been studied to make the luminosity constant during the spill [7].

3. SLHC Detector

3.1. Detector Upgrades for PHASE-I

A limited time of 6-8 months is available for installation in the shutdown in the year 2012/13. The ATLAS experiment plans to insert a new B-layer inside the current detector, along with a new smaller diameter beam pipe. The trigger and data acquisition system (TDAQ) will be continuously upgraded to cope with the increased rates and by taking advantage of new processing power. ATLAS is also looking at topological triggers, combining different trigger elements, e.g. muon with no jet, and a fast track finding scheme (associative memory) at Level-2 trigger.

3.2. Detector Upgrades for PHASE-II

Detectors for the SLHC must face two challenges: (1) pile-up events (a factor of 15-20 times LHC) and (2) radiation damage (a factor of 4-5 times LHC). Most of the ATLAS detector components will cope well at SLHC, e.g., magnet systems, muon systems, calorimeters, although some parts of these systems may need upgrading. The inner tracker, however, requires complete replacement. The radiation damage limit will have been reached and a finer granularity detector is required to cope with the pile-up events, e.g., for good pattern recognition.

B-layer & Outer Pixel-layers

The B-layer, with a radius as little as ~ 3.7 cm, will receive the fluence of $\sim 2.2 \times 10^{16}$ 1-MeV neutrons equivalent (neq)/cm², as discussed in the next section. The B-layer requires either a new sensor technology, e.g., 3D [9], Diamond [10], or a micro pattern gas detector such as GOSSIP [11], as an alternative, or replacement every few years. The outer pixel layers would extend up to the radius of ~ 30 cm or more, depending on the track finding performance for large pile-up events. The layers at radii larger than ~ 10 cm, the outer pixel layers, receive less than $\sim 4 \times 10^{15}$ 1-MeV neq/cm² and could be made with the current planar Silicon sensor technology. The large coverage area of the outer pixel layers will be a new challenge in reducing the unit production cost.

New Microstrip layers (SCT)

The radii larger than ~ 30 cm would be made with the silicon microstrip sensor technology, where the fluence will be less than 1×10^{15} 1-MeV neq/cm². Considerations include: the full depletion of the wafer may not be achieved; the wafer becomes p-type as the radiation damage in the silicon creates acceptor-like impurities; the large coverage area, radii from ~ 40 cm to ~ 100 cm, demands the minimum cost for the sensors. This leads to a logical choice of single-side-process sensors, compared with the double-side-process sensors, and of n-strip readout in p-bulk wafers, the n-in-p sensor. The n-in-p sensor has the readout junction always in the depleted region and collects electrons, the faster signal, in the Silicon. These not only eliminate signal loss due to under-depletion but also reduces ballistic deficit due to the faster signals.

With the much greater track density per beam crossing, 15-20 times more than the LHC, the length of the strip segment needs to be much shorter than the current length of 12 cm. If data transfer rate works up to occupancy of 2%, compared to the current 0.5%, a strip length of ~ 2.5 cm would be allowed.

The front-end ASIC's of both Pixels and Strips would be made with 130 or even 90 nm deep-submicron CMOS technology. Although they may have reduced the unit power per area, the total power would be large due to the high channel density. The temperature of the tracker needs to be lower by 15 °C in order to cope with similar heat generation in the damaged Silicon sensors to that of the LHC, thus, the coolant temperature would be around -40 °C. This demands a new cooling system, e.g., with a medium of CO₂. Taking into the consideration of the need for less material and the rapid installation in a short shutdown time, ATLAS is looking into the possibility of installing a complete inner tracker as one-piece.

3.3. Particle Fluence at SLHC

Particle fluences in the inner tracker of the ATLAS detector at LHC were studied extensively [8]. At LHC, the transition radiation tracker (TRT) works so as to moderate the neutrons to lower energies where their contribution to radiation damage is smaller. At SLHC, a polyethylene block of about 5 cm is proposed to perform a similar neutron moderation role. Particle fluences at SLHC at the integrated luminosity of 6,000 fb⁻¹, i.e., the nominal luminosity of 3,000 fb⁻¹ with a safety factor of 2, are shown in Fig. 1, extrapolated from the fluences at the ATLAS detector at LHC. The fluences correspond to those at the longitudinal location (Z) of about 150 cm.

The total fluence at a radius (R) of 4 cm, the location of the first pixel layer (the B-layer) would be about 2×10^{16} 1-MeV neutrons-equivalent (neq)/cm². At a radius of 30 cm, the location of the first microstrip layer (the first SCT layer) would be, the fluence is about 1×10^{15} 1-MeV neq/cm², reducing to about 7×10^{14} 1-MeV neq/cm² at a radius of 40 cm. Charged particles - pions and protons - dominate the fluence near the interaction point, decreasing as R⁻². Neutrons come both from the interaction point and from albedo (backsplash from the surfaces of the calorimeters), thus filling the inner detector volume more uniformly, dominating at radii larger than about 25 cm. Ionizing doses by the photons and charged particles are about 11, 0.5, and 0.3 MGy at radii of 4, 30, and 40 cm, respectively.

4. n-in-p Sensor Development in Japan and in ATLAS

Many groups have investigated n-in-p sensors for the SLHC [12]. The ATLAS collaboration has undertaken an R&D activity to develop non-inverting silicon strip detectors for the upgrade of the ATLAS inner tracker [13]. In Japan, an early n-in-p sensor was made in 1995 by manufacturing a microstrip sensor (p95) in a p-type wafer. Since 2005, new development of the p-type sensor was resumed for developing a highly radiation-tolerant silicon microstrip sensor for the SLHC application. To date, three generations have been made, the ATLAS05, ATLAS06, and ATLAS07 sensors, with wafer properties summarized in Table 2, and for the n-strip isolation method in Table 3. These sensors were fabricated in the silicon wafers commercially available to the vendor [14].

4.1. p95 p-type Sensors

A prototype n-in-p sensor was fabricated in p-type wafers of 100 mm diameter, 300 μm thick, Float Zone (FZ), crystal orientation of <111>, and resistivity of ~6 kΩ cm. The sensor was 6 cm long by 3 cm wide, with strip pitch of 50 μm, and with n-strip isolation by a common p-stop structure. The sensors were irradiated to 12 GeV protons up to the fluence of 1.1×10^{14} protons/cm² in 1995 [15] and one sensor to 3×10^{14} protons/cm² in 1996. The full depletion

voltages (FDV) were evaluated using the body capacitance vs. bias voltage (C-V) method. The sensors were re-measured after 10 years, in 2006, and still behaved well [16]. The sensors have been kept at 0 °C most of the time. The FDV's were ~220 V at the fluence of 1.1×10^{14} and ~360V at 3×10^{14} . The FDV of 1.1×10^{14} was ~340 V in 2006. The increase of FDV of ~120 V from 1995 to 2006 is consistent with the prediction for the n-type sensors by H. Ziock et al. [17].

4.2. ATLAS05 and ATLAS06 p-type Sensors

The ATLAS05 sensors were made to investigate the difference in silicon crystals and the n-strip isolation method in the 100 mm diameter silicon wafers. The FZ wafers came from the same lot as the p95 sensors. The other silicon crystal was of the Magnetic Czokralski (MCZ) method, shown to contain higher impurities such as Oxygen from the Silica crucible. The orientation of the crystal was also of interest in the investigation as the Si-SiO₂ interface trap density is an order smaller in the <100> than the <111> orientation [18]. The ATLAS05 sensors were made of miniature sensors of 1 cm x 1 cm with various isolation structures and a large sensor of 6 cm x 6 cm with 6 zones of isolation structures corresponding to those of the miniature sensors. The miniature sensors were named after the zone number in the large sensor. The layout of the sensors in the 100 mm wafer is shown in Fig. 2. The cross sections of the zones are shown in Fig. 3. The pitch of the strips was 80 μm.

The ATLAS06 sensors were made with 150 mm diameter, 320 μm thick p-type wafers: two types of FZ wafers, FZ-1 (higher grade: ~6.7 kΩ cm) and FZ-2 (lower grade: ~6.2 kΩ cm), and a MCZ (with a higher resistivity than the 100 mm wafer: ~2.3 kΩ cm). The 100 mm diameter process was becoming unavailable from the vendor, with more choices for the crystal and resistivity in the 150 mm diameter wafers. The wafer layout and the cross section of the zone structures of the ATLAS06 sensors are shown in Fig. 4 and Fig. 5, respectively.

4.3. Proton Irradiation at CYRIC

The miniature sensors of the ATLAS05 and ATLAS06 designs were irradiated at CYRIC [19] at Tohoku University, Sendai, Japan. The AVF Cyclotron provides protons to the beam lines with energy of 70 MeV, intensity of 10 nA - 800 nA, and beam spot size of ~7 mm full-width-half-maximum (FWHM). As the samples were larger than the beam spot, motorized stages moved the samples and scanned the area by $2 \times \sigma$ per side, where $\sigma = \text{FWHM}/2.35$.

The samples and the irradiation fluences are summarized in Table 4. The ATLAS05 sensors were irradiated to the fluence of $0.7 \times$ to 20×10^{14} 1-MeV neq/cm². The ATLAS06 sensors were to the fluence of $0.9 \times$ to 21×10^{14} 1-MeV neq/cm². The fluences were evaluated by using the activation of the Al foils. The irradiations were initially made in the 31-2 beamline and later in the 32 beamline due to conflict in user setups and machine time in the 31-2 beamline. The 31-2 beamline provides easier access to the irradiation area, whereas the 32 beamline, with straight beam extraction, has simpler beam tuning.

Results of the ATLAS05 sensors before and after the irradiations were published in [20], and those of the ATLAS05 and ATLAS06 sensors in [21]. Unless otherwise mentioned, the samples were annealed at 60 °C for 80 min to reach the minimum of full depletion voltage.

4.4. Full Depletion Voltage (FDV)

The FDV's of the sensors were evaluated from two parameters, the body capacitance (C) and the charge collection efficiency (CCE) for 1064 nm laser light, as a function of bias voltage (V). In the laser CCE-V method, although there seems uncertainty in the absolute values of the collected charges on a sample-by-sample basis due to yet unknown factors, the shape of the CCE-V plot allows extracting the FDV value. A large error should be associated in the extracted values in the high fluence samples as the FDV approached 1,000 V, the maximum bias voltage applied.

From the FDV's extracted with the laser CCE-V method (Fig. 12 of Ref. [21]), we observe,

(1) The increase of FDV (V_{fd}) as a function of fluence (ϕ), after the initial decrease, is approximately

$$V_{fd} \sim 100 \text{ [V]} + 35 \text{ [V/10}^{14} \text{ 1-MeV neq/cm}^2\text{]} * \phi \text{ [1-MeV neq/cm}^2\text{]} \quad (2)$$

in the ATLAS06 sensors, i.e., 150 mm wafers, independent of FZ-1, FZ-2, or MCZ.

(2) The ATLAS05 sensors, 100 mm wafers, gave distinctively different behavior: in the MCZ wafers, much larger FDV's were observed, by ≥ 100 V, than those of 150 mm wafers, although the slope of the increase of FDV is similar to the slope of the 150 mm wafers. The larger FDV could be attributed to the larger initial impurities as appeared as the low resistivity of ~ 0.9 k Ω cm.

The confirmation of the above observations requires further studies. There seems, however, no advantage to use the MCZ wafers from the FDV point of view.

4.5. Annealing

ATLAS06 sensors irradiated to 1.9×10^{14} 1-MeV neq/cm² were annealed at 60 °C in order to evaluate annealing and reverse annealing of the 150 mm p-type wafers. The evolutions of FDV as a function of time, $V_{fd}(t)$ were evaluated with the laser CCE-V method and are shown in Fig. 6. Also shown are the fits to the annealing formula given in Ref. [22],

$$V_{fd}(t) = V_a * (1 - \exp(-t/\tau_a)) + V_c + V_y * (1 - 1/(1 + t/\tau_y)) \quad (3)$$

where V_a and τ_a are the voltage and the time constant of the beneficial annealing, V_c the persistent voltage, and V_y and τ_y the reverse annealing voltage and the time constant, respectively. The τ_a and τ_y were fixed in the fits to the values, 24 min. and 1060 min., respectively, derived in the ref. which are the weighted average of mainly the n-type wafers. The parameter values obtained by the fits are listed in Table 5.

The time evolutions are well reproduced by the formula with the time constants of the n-type wafers; thus, these p-type wafers of FZ and MCZ are similar in defect character to the n-type wafers. The two FZ wafers are similar, with the FZ-2 having slightly more defects than the FZ-1 wafers. The MCZ wafers have much more defects than the FZ wafers. The FDV's at the minima are about 100 V lower than those of the non-annealed samples.

4.6. N-strip Isolation

The ATLAS05 and ATLAS06 sensors were fabricated without and with a p-spray process of indicative p-spray surface density of 2×10^{12} ions/cm². The indicative surface densities of p-stops were 5×10^{12} , 1×10^{13} and 2×10^{13} ions/cm². Thus, the miniature sensors of Zone1 in the p-spray wafers were p-spray only. Isolation of the n-strips can be achieved by depleting the

surface by applying bias voltage, if not achieved without the bias voltage. The bias voltage to achieve the isolation is defined by the bias voltage for which the current between the two adjacent n-strips, when a voltage of 5V is applied between them, reaches at value 10% larger than the asymptotic current at high bias voltages.

To compare isolation due to the wafer materials and to the isolation methods of p-stop or p-spray, the isolation bias voltages are shown in Fig. 7 for the ATLAS06 Zone3 (Z3) p-stop and the Zone1 (Z1) p-spray irradiated samples. In general, isolation was achieved at low fluences, and degraded as the fluence accumulated. This was unexpected as the density of the interface charges was expected to saturate. The samples achieved isolation at very low voltages up to 2×10^{14} 1-MeV neq/cm². The p-spray samples required higher bias voltages than those of the p-stop samples between the fluences of 5×10^{14} and 10×10^{14} 1-MeV neq/cm². At 2×10^{15} the difference disappeared. In regard to wafer materials, the isolation was better for MCZ than FZ-1 and FZ-2 in that order. From the samples of ATLAS05 and ATLAS06 sensors, the <100> orientation was better than the <111> orientation.

5. ATLAS07 p-type Sensors

The ATLAS07 sensors are designed in p-type 150 mm diameter wafers for two purposes: (1) to evaluate a large area silicon microstrip sensor, i.e., the maximum size from the wafer, 9.75 cm x 9.75 cm square sensor with 4 segments of 2.39 cm strip length each, for the intermediate radii of the inner tracker; (2) to provide 1 cm x 1 cm miniature sensors for characterization of the strip sensors and further evaluation of desirable features such as “Punch-through protection (PTP)” structures. PTP structures protect the AC coupling capacitors between the n-strip implant and the Aluminum metal over the implant against the shorting of the bulk by possible beam splash into the sensors. In the large area sensor design, two of the four segments are designed with "axial" strips where the strips are parallel to the sensor edges, and two with "stereo" strips where the strips are inclined to the sensor edges. The stereo strip segments are to identify and resolve design issues specifically associated with the layout. The wafer layout of the ATLAS07 sensor is shown in Fig. 8, and the structures of the miniature sensors are shown in Fig. 9. The wafer characteristics are summarized in Table 2 and the n-strip isolation method in Table 3. The strip pitch of the ATLAS07 sensor was 74.5 μ m, constrained by the number of channels available from ten readout ASIC's with 128 channels per chip. As of this publication, only the FZ-1 wafers have been fabricated.

5.1. ATLAS07 Proton and Neutron Irradiations

A set of samples of ATLAS07 miniature sensors was irradiated with 70 MeV protons at CYRIC to fluences of 2.3x, 6.0x and 13x 10^{14} 1-MeV neq/cm². Another set was irradiated to the reactor neutrons at the TRIGA reactor to 2x, 5x and 10x 10^{14} 1-MeV neq/cm². The fluence of 1-MeV neq/cm² was calculated by integrating the non-ionizing-energy-loss (NIEL) damage factors [23] for the energy spectrum of neutrons in the reactor extending up to ~5 MeV [24].

Charge collection in the irradiated ATLAS07 sensors was evaluated with the beta rays from ⁹⁰Sr at institutes of the ATLAS Upgrade Silicon Detector R&D collaboration [25]. The collected charges for proton irradiation to 1.3×10^{15} 1-MeV neq/cm² is shown in Fig. 10 and for the neutron irradiations to null, 5×10^{14} , and 1×10^{15} 1-MeV neq/cm² in Fig. 11. The samples measured were not annealed unless otherwise mentioned. The FDV of the proton samples could be around 800 V, consistent with ~700 V after the annealing at 60 °C for 80 min, as

described in section 4.4 for the laser CCE-V method. The collected charges also improved by about 15% after the annealing. The radiation damage apparent from the charge collection seems worse for neutrons than for protons for the fluence scaled by the NIEL factor. The collected charge at bias voltage of 500 V is estimated to be ~15k electrons (e's) for protons and ~10k for neutrons at fluence of 1×10^{15} 1-MeV neq/cm², resulting in a expected charge of ~12k e's for damage from a 50-50 mixture of charged particles and neutrons. Further results and compilation of the collected charges are presented in this conference [26].

5.2. ATLAS07 Improvement

Evaluation of the ATLAS07 miniature and large area sensors has revealed several weak spots on the sensors that lead to onset of microdischarge at low bias voltages. Identification of the weak spots by hot-electron analysis and by semiconductor technology CAD (TCAD) simulations identified the potential causes associated with the p-stop designs [27]. Improved sensors, ATLAS07-II, have been subsequently fabricated. The leakage current behavior of the ATLAS07-II miniature sensors with p-stop concentration of 4×10^{12} ions/cm² is shown in Fig. 12. The onset voltage of microdischarge has been successfully increased to over 1,000 V. The onset of the microdischarge in the large area sensors remains to be confirmed. In both the ATLAS07 and ATLAS07-II sensors, the n-strips were isolated from as low bias voltage as 10 V, prior to irradiation. An exception was the Zone1 with no isolation implantation which required a high bias voltage.

5.3. ATLAS07 Large Area Sensor

A few large area sensors of the ATLAS07 were characterized for strip yield and for inter-strip capacitance with a bias voltage of 50 V. The strip yield was 99.95%. The interstrip capacitance measured at a frequency of 100 kHz was 0.75 pF/cm for the nearest neighbors, i.e. the capacitance between the adjacent strips. For two-neighbors on either side, the capacitance was 10-15% larger [28].

6. Summary

In order to explore the physics potential of the LHC, the LHC accelerators and detectors will be upgraded in two phases, PHASE-I and PHASE-II. PHASE-I is to start around 2013 with peak and average luminosities of $3 \times$ and 1.7×10^{34} cm⁻²s⁻¹ respectively. PHASE-II, the SLHC, is to start around 2017 with luminosities of $\geq 10 \times$ and 3.6×10^{34} cm⁻²s⁻¹, respectively. The ATLAS and the CMS detector each will collect proton-proton collision data of ~ 700 fb⁻¹ by the end of PHASE-I, and ~ 3000 fb⁻¹ by the end of PHASE-II. The physics motivations to verify the Higgs potential and new physics beyond the standard model are expected to be justified in a few years from the start-up of LHC.

The complete inner trackers of the ATLAS detector will be replaced for the PHASE-II operation. The inner tracker will consist mainly of Silicon, with Silicon pixels in the inner part (the radius, R, below ~ 30 cm) and with Silicon microstrip detectors in the outer part (~ 30 cm $< R < 110$ cm) for the granularity of the position-sensitive elements required. Radiation tolerance is the key issue. The contribution of neutrons to the particle fluence in the tracker becomes significant in the SLHC, $>50\%$ at $R > 30$ cm. In the Silicon microstrip detectors community, the n-strip in p-type material, n-in-p, microstrip sensors have been developed extensively for several years in Europe and in Japan. The n-in-p sensor collects electrons, the

faster signals, generated by the passage of the charged particles in the p-n junction side throughout the radiation damage lifetime of the detector.

Characterization of FZ and MCZ wafer materials were made in the ATLAS05 and ATLAS06 sensors. Design details have been advanced through the development of ATLAS05, ATLAS06, and ATLAS07 sensors. Although further development is required to finalize all desirable features, an n-in-p Silicon microstrip sensor has emerged that tolerates sensor operation up to the bias voltage of $\sim 1,000$ V, collects signals of $\geq 12k$ e's at 500 V at fluence of 1×10^{15} 1-MeV neq/cm², and can be made from the 150 mm diameter FZ wafers commercially available in industry.

7. Acknowledgement

The work in Japan is supported partly by the Grant-in-Aid for Scientific Research (A), 20244038, of the Japan Society for the Promotion of Science (JSPS).

References

- [1] CERN Press Release PR08.08E, <http://press.web.cern.ch/press/PressReleases/Releases2008/PR08.08E.html>.
- [2] CERN Press Release PR17.08E, <http://press.web.cern.ch/press/PressReleases/Releases2008/PR17.08E.html>.
- [3] F. Gianotti et al., Eur.Phys.J. C39 (2005) 293-333, (DOI) 10.1140/epjc/s2004-02061-6.
- [4] CERN Council, "The European strategy for particle physics", CERN/2685, <http://council.web.cern.ch/council/en/EuropeanStrategy/ESParticlePhysics.html>.
- [5] L. Evans, "SLHC accelerator and injector upgrades", SLHC-PP kickoff meeting, <http://indico.cern.ch/conferenceOtherViews.py?view=standard&confId=29254>.
- [6] W. Scandale, F. Zimmerman, "Scenarios for sLHC and vLHC", care-hhh.web.cern.ch/care-hhh/Literature/hcp2007.pdf.
- [7] J. P. Koutchouk, G. Sterbini, K. Ohmi, "Increasing the integrated luminosity of SLHC by luminosity leveling via the crossing angle", Proceedings of EPAC08, Genoa, Italy, care-hhh.web.cern.ch/care-hhh/Literature/EPAC8/wepp013.pdf.
- [8] S. Baranov et al., "Atlas Radiation Background Task Force Summary Document", ATL-GEN-2005-001.
- [9] 3D: e.g., C. Kenney et al., IEEE Trans. Nucl. Sci. 46 (1999) 1224-1236.
- [10] Diamond: e.g., J.J. Velthuis et al., Nucl. Instr. Meth. A591 (2008) 221-223.
- [11] GOSSIP: e.g., M. Campbell et al., Nucl. Instr. Meth. A560 (2006) 131-134.
- [12] Liverpool: G. Casse et al., Nucl. Instr. Meth. A487 (2002) 465-470, RD50: G. Casse et al., Nucl. Instr. Meth. A518 (2004) 340-342.
- [13] H.F-W. Sadrozinski, "Development of non-inverting Silicon strip detectors for the ATLAS ID upgrade", https://edms.cern.ch/file/816759/1/ATLAS_RD_SSD_May_18_06.doc.
- [14] Hamamatsu Photonics K.K., 1266 Ichino-cho, Hamamatsu-shi 435-8558, Japan.

- [15] S. Terada et al., Nucl. Instr. Meth. A383 (1996) 159-165.
- [16] K. Hara et al., Nucl. Instr. Meth. A565 (2006) 538-542.
- [17] H. Ziock et al. Nucl. Instr. Meth. A342 (1994) 96.
- [18] S. M. Sze, Physics of Semiconductor Devices, Second ed., Wiley, New York, p. 386.
- [19] Cyclotron Radio Isotope Center (CYRIC), 6-3 Aramaki-Aoba, Aoba-ku, Sendai 980-8578.
- [20] Y. Unno et al., Nucl. Instr. Meth. A579 (2007) 614-622.
- [21] K. Hara et al., 2007 IEEE Nucl. Scie. Symp. Conference Record, 1 (2007) 633-638, and submitted for publication in IEEE Trans. Nucl. Scie.; K. Hara et al., 2008 IEEE Nucl. Scie. Symp., Dresden, Conference record, (2008) N19-2.
- [22] M. Moll, Thesis, University of Hamburg, 1999.
- [23] A. Vasilescu (INPE Bucharest) and G. Lindstroem (University of Hamburg), Displacement damage in silicon, on-line compilation, <http://sesam.desy.de/members/gunnar/Si-dfuncs.html>.
- [24] I. Mandic, <http://www-f9.ijs.si/~mandic/Reactor.html>.
- [25] Institutes: University of Liverpool (LIV), Jozef Stefan Institute (LJUB), University of California, Santa Cruz (UCSC).
- [26] A. Affolder et al., this conference.
- [27] Y. Unno et al., 2008 IEEE Nucl. Scie. Symp., Dresden, Conference record: N30-378.
- [28] B. Hommels, measured at University of Cambridge.

Table 1. Comparison of the schemes of the interaction point of the SLHC and LHC

	LHC	PHASE-I	ES	FCC	LPA
N_b [10^{11} particles/bunch]	1.15	1.7	1.7	1.7	4.9
n_b	2808	2808	2808	2808	1404
β^* [cm]	55	25	8	8	25
Collision angle [μ rad.]	285	285	0	0	381
F	0.86	0.86	1	1	0.45
Peak L [10^{34} $\text{cm}^{-2}\text{s}^{-1}$]	1	3	15.5	15.5	10.7
$\langle L \rangle_{10 \text{ hrs}}$ [10^{34} $\text{cm}^{-2}\text{s}^{-1}$]	0.46	--	2.4	2.4	2.5
Peak pile-up [events/crossing]	19	--	294	294	403

Table 2. Wafer properties of the p-type sensors

	Wafer diameter [mm]	Wafer thickness [μ m]	Crystal growth	Crystal Orientation	Resistivity [$\text{k}\Omega$ cm]
p95	100	300	FZ	$\langle 111 \rangle$	~ 6
ATLAS05	100	300	FZ	$\langle 111 \rangle$	~ 6
	100	300	MCZ	$\langle 100 \rangle$	~ 0.9
ATLAS06	150	320	FZ1	$\langle 100 \rangle$	~ 6.7
	150	320	FZ2	$\langle 100 \rangle$	~ 6.2
	150	320	MCZ	$\langle 100 \rangle$	~ 2.3
ATLAS07	150	320	FZ1	$\langle 100 \rangle$	~ 6.7
	150	320	FZ2	$\langle 100 \rangle$	~ 6.2

Table 3. N-strip isolation method and surface concentration [ions/cm^2]

	p-stop	p-spray + p-stop	p-spray
p95	2×10^{13} , 1×10^{14}	--	--
ATLAS05	1×10^{13} , 2×10^{13}	$2 \times 10^{12} + 2 \times 10^{12}$	2×10^{12}
ATLAS06	5×10^{12} , 1×10^{13} , 2×10^{13}	$2 \times 10^{12} + 2 \times 10^{12}$	2×10^{12}
ATLAS07	2×10^{12} , 4×10^{12}	$2 \times 10^{12} + 2 \times 10^{12}$	2×10^{12}

Table 4. Irradiations of ATLAS05, ATLAS06, and ATLAS07 sensors

	Particle	Irrad. site	Exp. No.	Date (yy/mm/dd)	Beam line	Fluences [10^{14} 1-MeV neq/cm ²]
ATLAS05	p70 MeV	CYRIC	8512	06/06/26	31-2	0.7, 7
ATLAS05	p70 MeV	CYRIC	8512	06/10/16	31-2	1.1, 1.9, 5.5, 11, 20
ATLAS06	p70 MeV	CYRIC	8705	07/05/18	31-2	5.1, 10, 21
ATLAS06	p70 MeV	CYRIC	8705	07/08/28	32	0.9, 1.8
ATLAS07	p70 MeV	CYRIC	8705	08/03/11	32	2.3, 6.0, 13
ATLAS07	n Reactor	TRIGA	--	08/04/18	Small	2, 5, 10

Table 5. Fitted parameters of the annealing of the ATLAS06 sensors irradiated to 1.9×10^{14} 1-MeV neq/cm²

	τ_a [min]	τ_v [min]	V_a [V]	V_c [V]	V_v [V]
FZ-1	24 (*)	1060 (*)	96	94	418
FZ-2	24 (*)	1060 (*)	141	116	440
MCZ	24 (*)	1060 (*)	179	124	824

(*) These parameters are fixed to the values listed in the fitting.

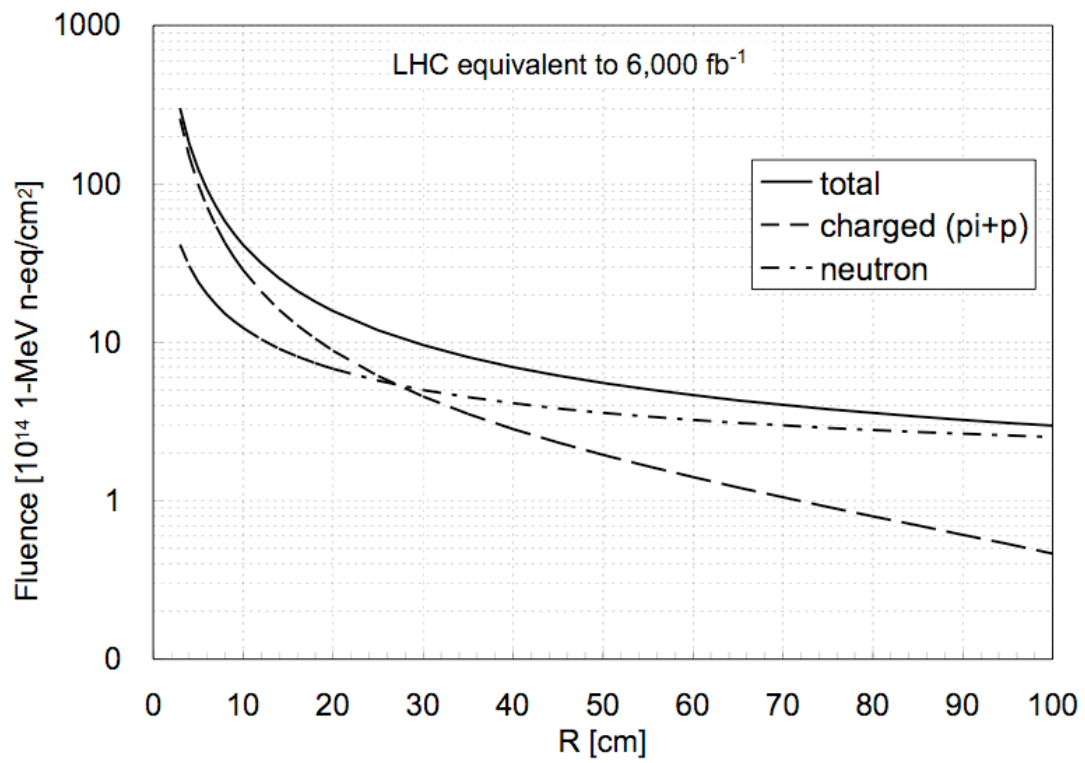


Fig. 1 Particle fluences expected in the inner detector of the ATLAS detector at SLHC.

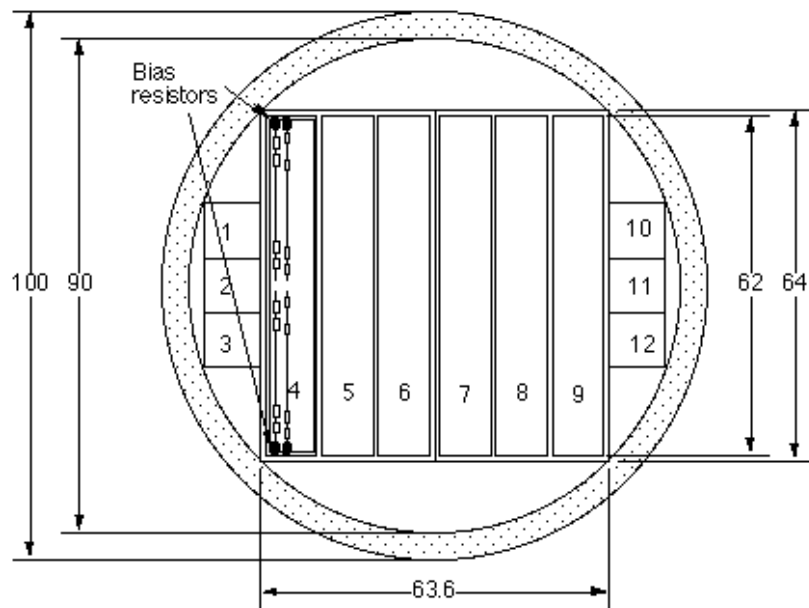


Fig. 2 Wafer layout of the ATLAS05 p-type sensors.

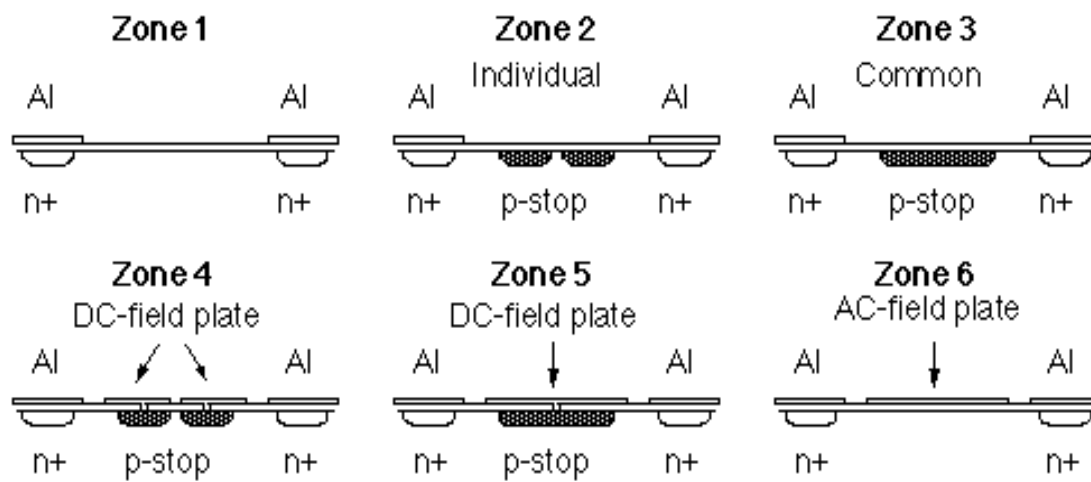


Fig. 3 Cross-sections of the strip side of the ATLAS05 p-type sensors, in the zones of the n-strip isolation structures.

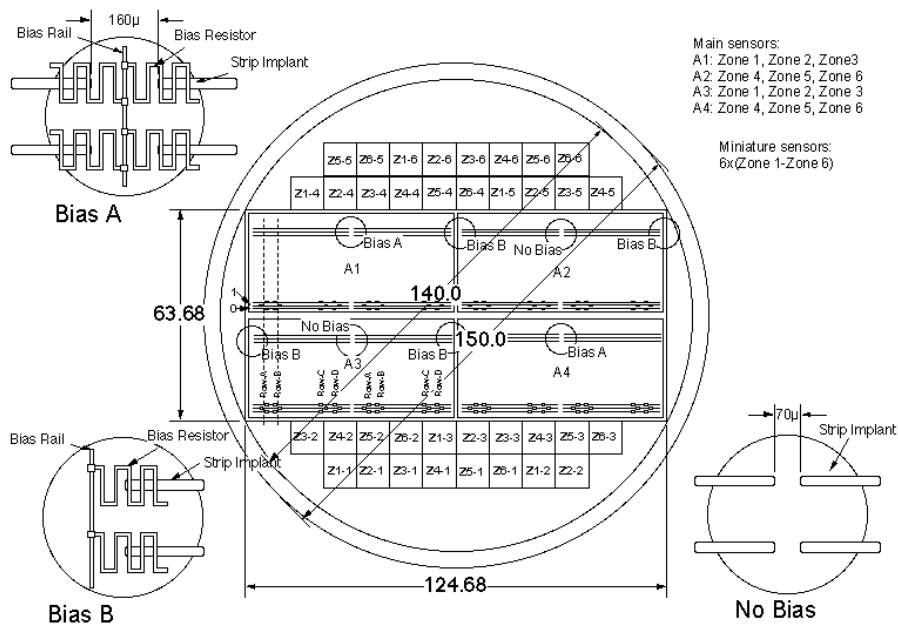


Fig. 4 Wafer layout of the ATLAS06 p-type sensors. The large area sensors have two segments of strips in a sensor, together with two bias resistor arrangements.

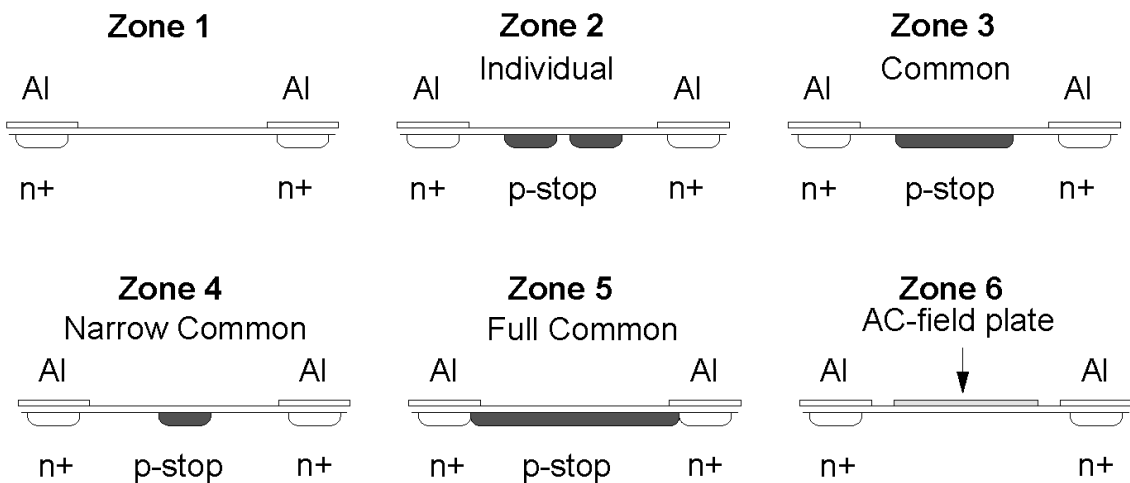


Fig. 5 Cross-sections of the strip side of the ATLAS06 p-type sensors with the zone names.

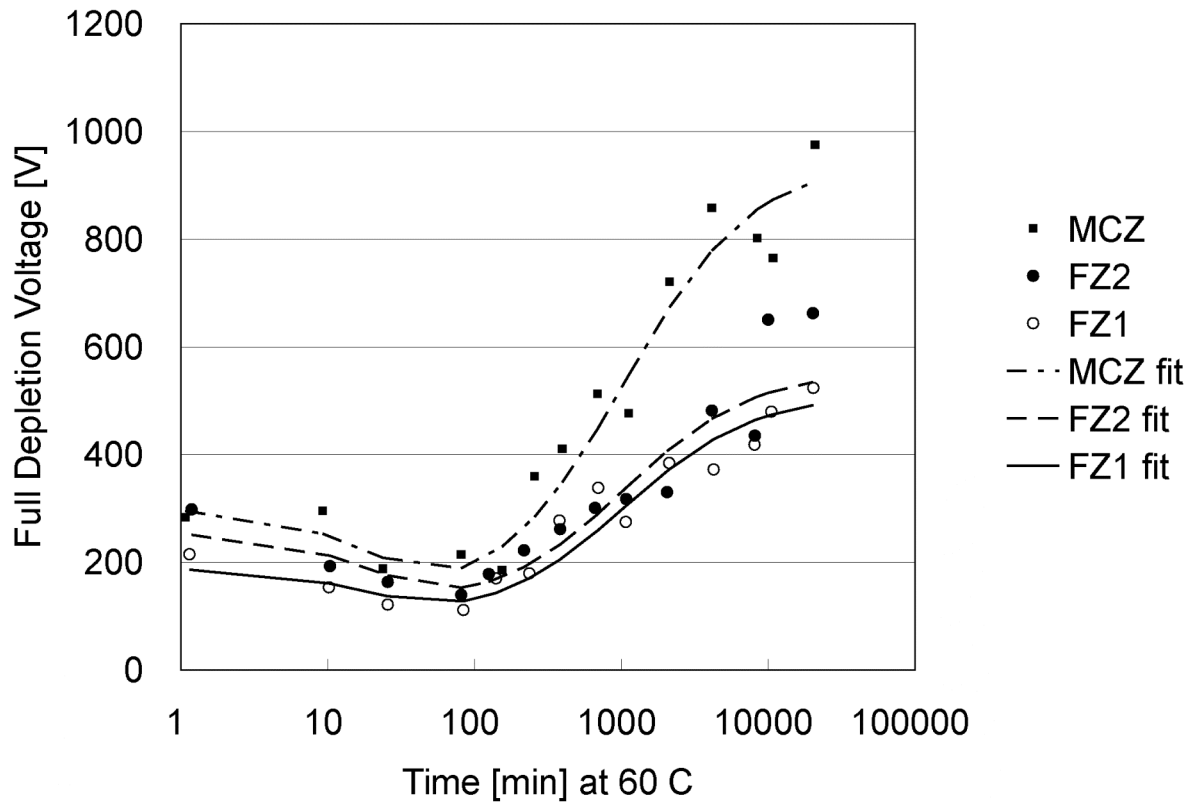


Fig. 6 Annealing at 60 °C of the ATLAS06 sensors irradiated to 1.9×10^{14} 1-MeV neq/cm². The full depletion voltages were estimated with the laser CCE-V method. The fits are made with the annealing formula and the time constants of 24 min. for the short-term and 1060 min. for the reverse annealing in Ref. [22].

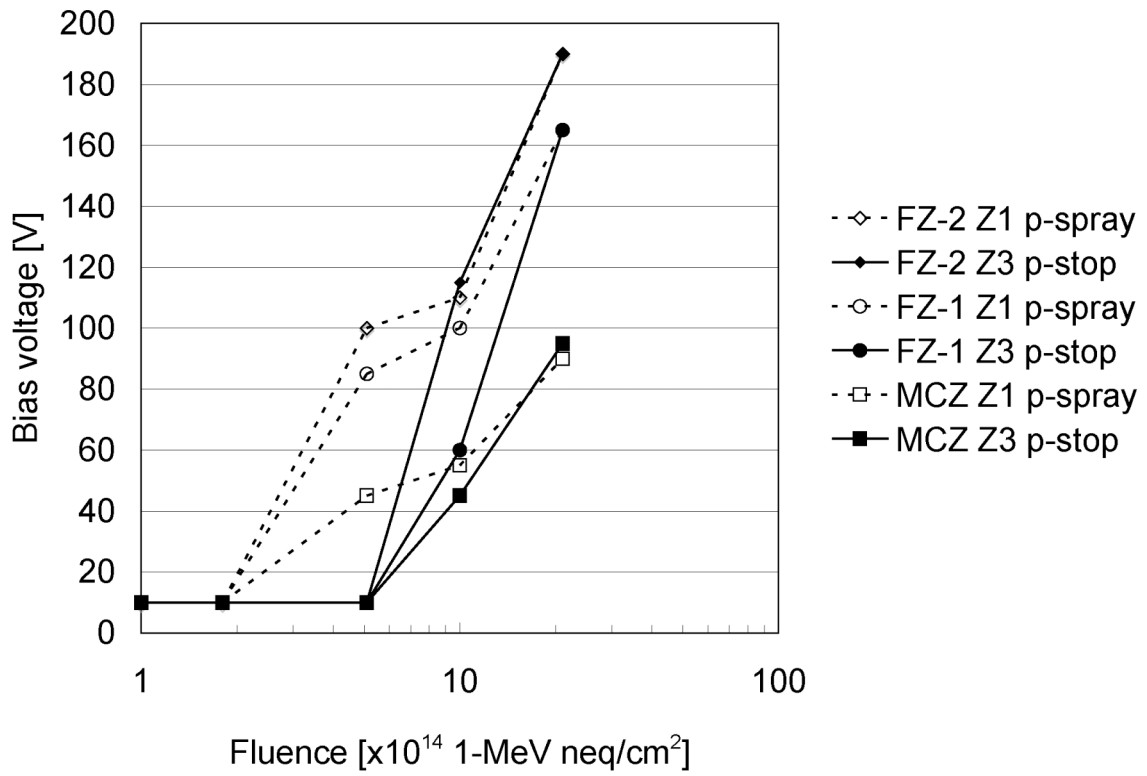


Fig. 7 Bias voltages to achieve n-strip isolation in the ATLAS06 sensors irradiated.

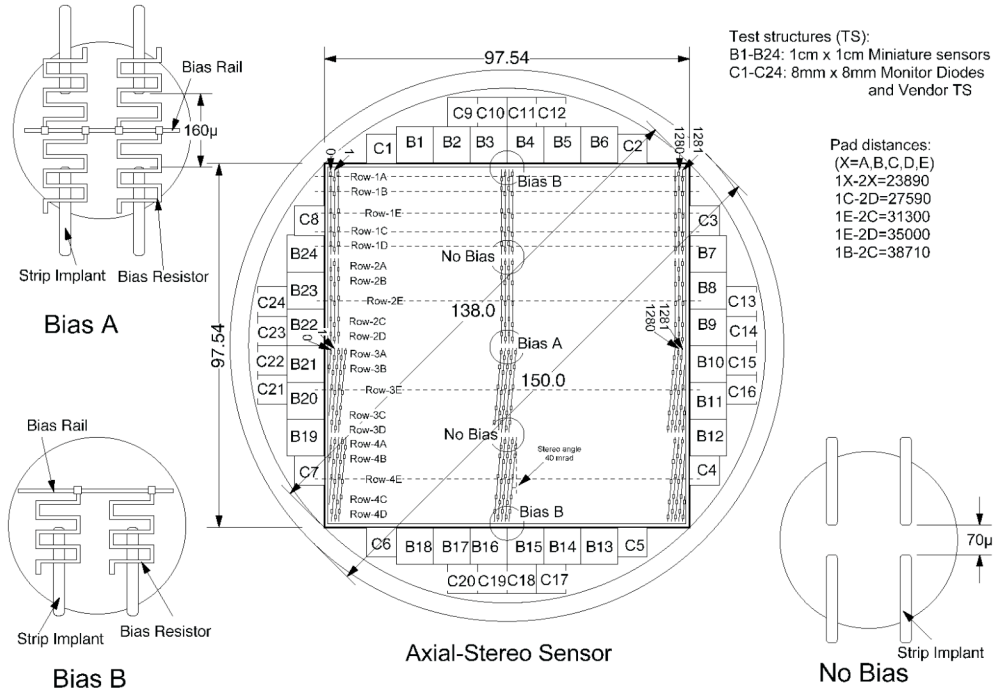


Fig. 8 Wafer layout of the ATLAS07 p-type sensors. The large area sensor has 4 segments of strips: top two with axial strips and the bottom two with stereo strips.

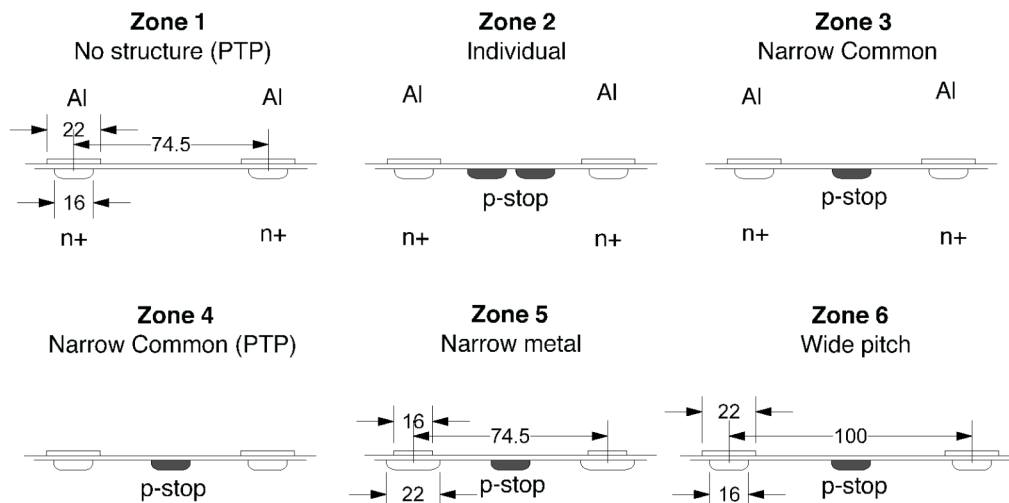


Fig. 9 Cross-sections of the strip side of the ATLAS07 p-type sensors of the zone names.

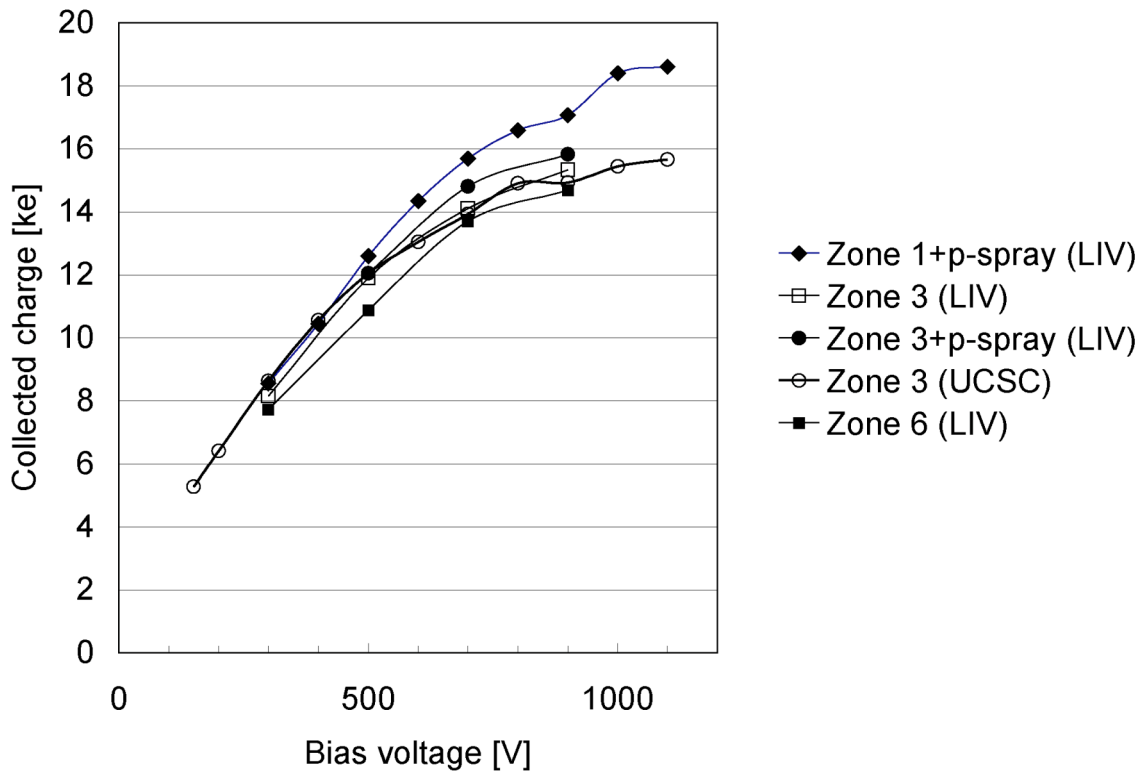


Fig. 10 Charge collection in the ATLAS07 sensors irradiated to 70 MeV protons to the fluence of 1.3×10^{15} 1-MeV neq/cm². The samples were not annealed.

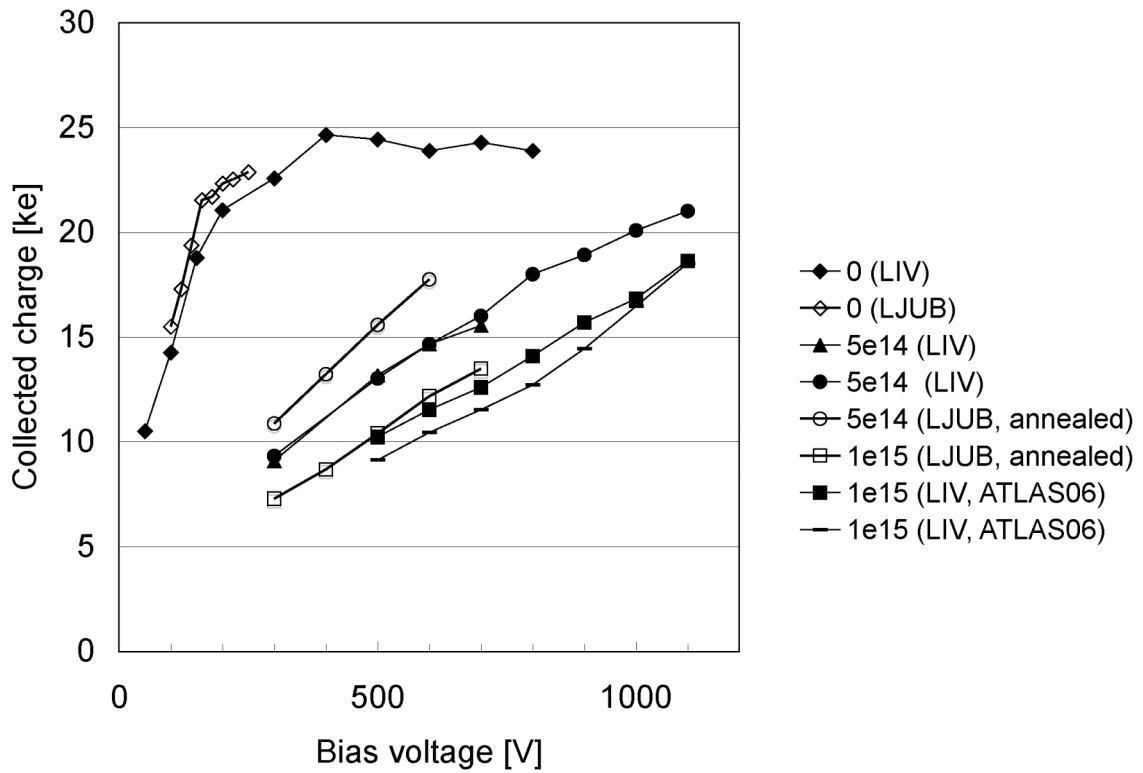


Fig. 11 Charge collection in the ATLAS07 and ATLAS06 sensors irradiated to neutrons to the fluences of 5×10^{14} and 1×10^{15} 1-MeV neq/cm². The samples were not annealed otherwise mentioned.

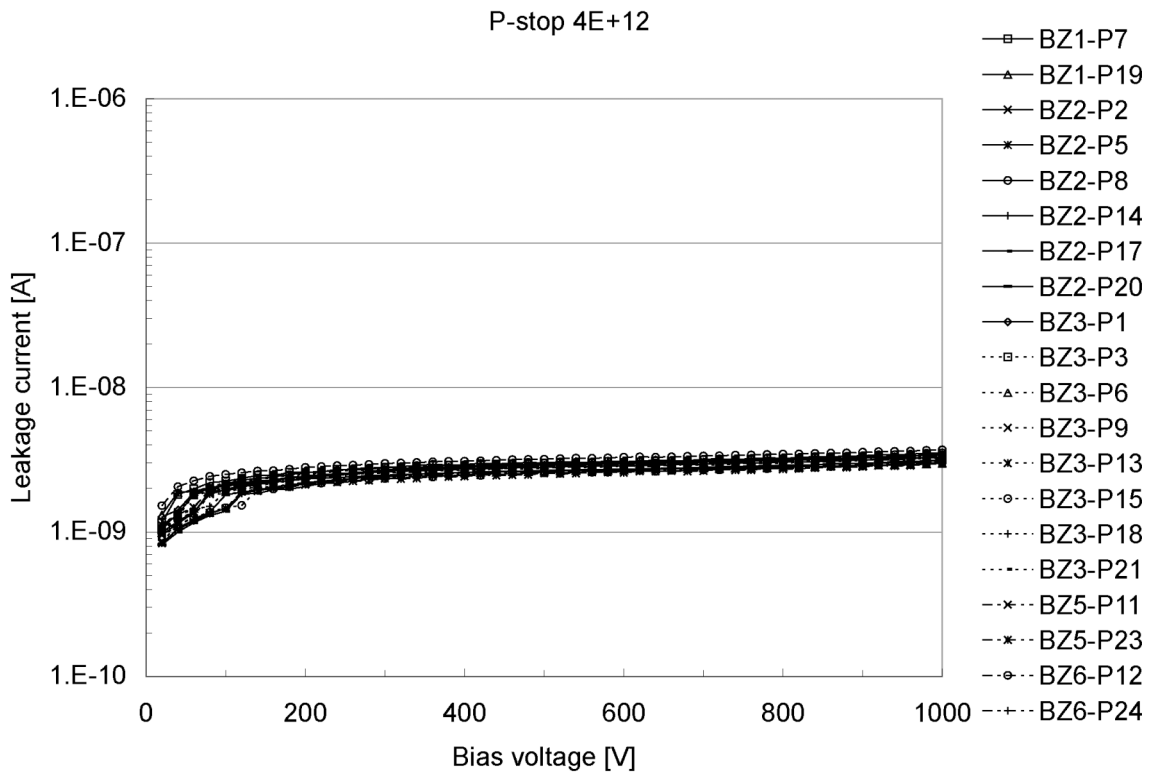


Fig. 12 Leakage current behavior of the ATLAS07-II miniature sensors after improvement. The irregularity seen below about 100 V was due to the equipment feature.